19th Brazilian Congress of Thermal Sciences and Engineering
November 6th–10th, 2022, Bento Gonçalves - RS - Brazil

ENC-2022-0062
COMBUSTION-TURBULENCE INTERACTION AND ENGINE PERFORMANCE: A CRFD NUMERICAL SIMULATION ON DIRECT-INJECTION SPARK-IGNITION ENGINES

Gabriel de Andrade Janene Gonini
gabriel.gonini@labmci.ufsc.br
Javier Antonio Mendoza Corredor
javier.mendoza@labmci.ufsc.br
Milton Keisy Kouketsu
milton.kouketsu@labmci.ufsc.br
Miguel Humberto Barrientos Sandoval
miguel.sandoval@labmci.ufsc.br
Leonel R. Cancino
leonel.cancino@labmci.ufsc.br
Internal Combustion Engines Laboratory - Joinville Technological Center - Federal University of Santa Catarina - LABMCI/CTJ/UFSC. Rua Dona Francisca 8300, Joinville, SC, Brazil, CEP 89219-600
Amir Antonio Martins Oliveira Jr.
amir.oliveira@ufsc.br
Combustion and Thermal Systems Engineering Laboratory - Mechanical Engineering - Federal University of Santa Catarina - LABCET/EMC/CTC/UFSC, Bairro Trindade, Florianópolis, SC, CEP 88040-900, Brazil.

Abstract. *Fuel direct injection (DI) is not a new technology, but its importance has been increasing in recent developments of spark ignition (SI) internal combustion engines (ICE). The development of this and other ICE technologies is better assisted with computational reactive fluid dynamics (CRFD) simulations. The present work assesses a CRFD DI-SI ICE model for combustion and engine performance purposes, more specifically, analyzing the turbulence-combustion interaction. The baseline simulation is one from AVL FIRE's database. It takes into account combustion, species transport, emissions, spray behavior, and wall-film models. The extended coherent flame model (ECFM-3Z) combustion model (3 zones) was used with the Discrete Droplet Model (DDM) spray model. The coherent flame model is based on a laminar flamelet approach, in which flame velocity and thickness are mean values integrated along the flame front, only dependent on the pressure, the temperature, and the stoichiometry of the unburned gases. As such, it decouples chemistry and turbulence; however, the variation on the turbulence model is expected to promote some changes in flow and chemical species fields, which influence the flamelet position and, therefore, the rate of heat release. To assess the influence of the turbulence model, the baseline case is compared to modified cases, changing the turbulence model from $k-\zeta-f$ to $k-\varepsilon$, for different engine rotations. This led to differences on tangible quantities of interest that evaluate the engine performance and characterize combustion (torque, power, mass fraction burnt and combustion duration). Also, quantities like pressure, temperature, rate of heat release and normalized turbulence intensity aid the comparisons.*

Keywords: *Combustion models, Direct-Injection Spark-Ignition Internal Combustion Engines, AVL-FIRE™ , Turbulence models, Turbulence-Combustion Interaction*

1. INTRODUCTION

Fuel direct injection (DI) is not a new technology, but its importance has been increasing in recent developments of spark ignition (SI) internal combustion engines (ICE). The fuel is directly sprayed at high pressures in the cylinder, promoting a cooling effect, a higher engine compression, and a consequent efficiency increase (Robert Bosch GmbH, 2022). In essence, with the same compression ratio as in manifold or port fuel injection (PFI), the compression temperature and resultantly the knocking sensitivity would be reduced; however, this cooling effect is normally used to increase the compression ratio with the same knocking sensitivity (Merker *et al.*, 2012). In the automotive industry, the development

of this and other ICE technologies is better assisted with computational reactive fluid dynamics (CRFD) simulations.

Combustion models are responsible for simulating species depletion and formation, ignition and combustion of fuel/air mixtures and their exhaust gases. Besides, the mean chemical reaction rates are usually non-linear functions dependent upon the local values of temperature and species concentrations and, therefore, are hard to determine (AVL List GmbH, 2021b). Detailed chemical kinetics mechanisms are currently computationally expensive due to the number of species and the consequent number of transport equations. On the other hand, a single-step irreversible reaction is too simple to represent hydrocarbon. Combustion models such as the Coherent Flame Models (CFM) balance much better this problem, with a combination of more complex oxidation schemes, composed of some reaction steps and some equilibrium reactions (AVL List GmbH, 2021b).

The CFM family assumes that the chemical time scales are much smaller than the turbulent ones, a plausible assumption for reciprocating ICEs (AVL List GmbH, 2021b). Thus, it is possible to apply a laminar flamelet approach, in which flame velocity and thickness are average values integrated along the flame front, only dependent on pressure, temperature, and stoichiometry of the unburned gases (AVL List GmbH, 2021b). As such, it decouples chemistry and turbulence; however, the variation on the turbulence model is expected to promote some changes in flow and chemical species fields, which influence the flamelet prediction and, therefore, the rate of heat release. Thus, the present work assesses a CRFD DI-SI ICE model for combustion and engine performance purposes, more specifically, analyzing the turbulence-combustion numerical interaction.

2. THEORETICAL BACKGROUND ON COMPUTATIONAL MODELS

This section describes a brief review on the models that most affect the ICE simulation, namely, combustion, turbulence and spray models. Other details of the simulation are more straightforwardly described in the next section, as the baseline case is one from AVL FIRE's database.

2.1 Combustion modeling

The Extended CFM (ECFM) has been mainly developed for DI-SI engines. While port fuel injection (PFI) SI engines run under homogeneous conditions, DI-SI may run under very stratified conditions (Colin *et al.*, 2003). This way, spark ignition, combustion and pollutants effects need to account for both average flow quantities and their fluctuations. The large scale stratification is described by local values of unburnt equivalence ratio, burnt and unburnt gases composition and temperature. Additionally, the small scale stratification is included via a variance/scalar dissipation model in combination with a presumed probability density function (PDF) for the fuel stratification (Colin *et al.*, 2003).

The ECFM differs from CFM because the CFM developed by Duclos *et al.* (1996) does not consider exhaust-gas recirculation (EGR) within the fresh gases composition. This way, the fresh gases temperature is estimated using a polytropic compression law. To cope with stratification, Duclos and Zolver (1998) introduced the fuel and oxygen tracers which allow to compute locally the fresh gases composition even in the presence of EGR. Conversely, their fresh gases enthalpy equation computes precisely the fresh gases temperature (Colin *et al.*, 2003).

Since the fresh gases state is more accurately predicted, the local laminar flame speed (LFS) is better predicted as well. Furthermore, for the CFM-type models, the reaction rate is proportional to LFS. Hence, the ECFM is expected to describe better the fresh gases and better account for large scale stratification effect on combustion (Colin *et al.*, 2003). With respect to small scale stratification, the average equivalence ratio used to calculate the LFS may lead to deviations. In short, this problem is solved by applying a PDF for the fuel mass fraction and then substituted in the LFS integration (or interpolation, for faster calculation) to yield a statistical average LFS.

To summarize, the ECFM couples combustion with spray modeling to allow stratified combustion, EGR and NO modeling (AVL List GmbH, 2021b). On top of that, the 3-Zones Extended Coherent Flame Model (ECFM-3Z) is a combustion model that works with all combustion modes (autoignition, propagation flame and diffusion flame) without knowing which one might take place beforehand (Colin and Benkenida, 2004). This is particularly important as autoignition may occur in SI ICEs as the undesirable knock. In fact, some knock considerations were already present in the ECFM formulation of Colin and Benkenida (2004), as they argue that the fresh gases state has to be defined accurately to yield a correct estimation of the laminar flame characteristics and of the autoignition delay time for a correct prediction of knock and detail this modeling.

The state of the gas mixture is described by a 2D space of mixture fraction and reaction progress ($Z, \tilde{c}$). Regarding Z, it is described by a probability density function (PDF) and each computational cell is divided into three mixing zones: the unmixed fuel zone, the mixed zone containing fuel, air and EGR, and the unmixed air plus EGR zone. Regarding $\tilde{c}$, it is null for unburnt gases and unity for completely burnt gases (Colin and Benkenida, 2004). In essence, this combustion model is based on a flame surface density transport equation and a mixing model that describes the three combustion modes (AVL List GmbH, 2021b).

2.2 Turbulence modeling

A near-wall turbulent flow can be divided into a inner region that scales on a viscous length and an outer region that scales on a flow length. The wall-bounded turbulent shear flow ought to be correctly modelled to capture turbulent quantities in this inner region. The blocking caused by a wall is governed by a elliptical partial differential equation; hence, non-local effects in non-homogeneous turbulent flows should consider an elliptical model. Moreover, the damping factors are artificial manoeuvres to represent the kinematic constraints caused by blocking (Durbin, 1991).

The $\overline{v^2} - f$ model proposed by Durbin (1991) eliminates empirical damping functions and accounts for some near-wall anisotropic turbulent effects, modelled through the elliptic relaxation function f (note that this adds a differential equation to the problem, however). This way, it is a better option than $k - \varepsilon$ and similar models that only consider isotropic turbulence and use damping terms. $k - \varepsilon$ limitations are largely due to the turbulence being represented by its kinetic energy (k), which is a scalar. As such, it may not reflect differences in the energy components ($\overline{u^2}, \overline{v^2}, \overline{w^2}$) that are produced by external forces with different component magnitudes (Durbin and Reif, 2010). Yet, these models are still inferior to second-moment (such as Reynolds Stress Models, RSM) and advanced non-linear eddy viscosity models when used in three-dimensional flows, with strong secondary recirculation, rotation and swirl (Durbin, 1991), typical of ICE CFD simulations.

However, the main computational inefficiency of the $\overline{v^2} - f$ model is its f wall boundary condition (f_w) sensitiveness, proportional to y^{-4}. Due to this exponent, it suffers with small y^+, contrary to most near-wall models. The $k-\zeta-f$ model proposed by Hanjalić *et al.* (2004) is an upgrade of the previous model and overcomes this problem by solving a transport equation for ζ instead of $\overline{v^2}$. $\overline{v^2}$ is a wall-normal velocity scale; ζ is a normalization of this variable ($\zeta = \overline{v^2}/k$), but also regarded as the ratio of the two time scales: lateral $\overline{v^2}/\varepsilon$ (anisotropic), and scalar k/ε (isotropic) (CFD Online, 2014). Note that ζ is still a scalar (the problem of k) but this time it is a scalar measure of anisotropy. The main improvement is that ε no longer appears on the $\overline{v^2}$ equation and its role is reproduced by the turbulent kinetic energy production (P_k) in the ζ equation. Essentially, the problem switches from a calculation of a variable (ε) that is dependent upon near-wall treatment to a variable (P_k) that is dependent upon the local turbulent stress and the mean velocity gradient capture, the goal of turbulence closure models (Hanjalić *et al.*, 2004). Moreover, the model formulates a more robust f_w boundary condition, this time proportional to y^{-2} and not y^{-4}.

The $k - \varepsilon$ model is by no means a weak model. It has been extensively tested, it is numerically robust and arguably the most used turbulence model in CFD codes. The model may have its limitations but it is generally considered to yield reasonable predictions of major mean-flow features. Thus, it is suitable for the current case, where modelling other physical phenomena, such as chemical reactions, combustion, multiphase interactions, brings in uncertainties that outweigh those inherent in the $k - \varepsilon$ turbulence model (AVL List GmbH, 2021a). For this reason, it is the chosen model for the variation case, to analyze the turbulence-combustion interaction.

Besides, more demanding models were tested and diverged, as they would require finer meshes. These models are the AVL hybrid turbulence models (HTM 1 and HTM 2), which are a hybrid between $k - \varepsilon$ and RSM, the RSM model itself, and a low-Reynolds model, represented by $k - \varepsilon$ with the near-wall approach as the wall treatment. Therefore, the chosen turbulence models are the $k - \zeta - f$ and the $k - \epsilon$ models, both using the hybrid wall treatment, that is a generalized treatment that ensures a gradual change between viscous sub-layer and the wall functions, where the integration of the equations occur for small values of y^+ and the standard wall function takes place for the large values of y^+ (AVL List GmbH, 2021a).

2.3 Spray modeling

The spray is modeled in a Lagrangian multiphase approach. More precisely, the Discrete Droplet Model (DDM) treats the Lagrangian particles and the Eulerian flow in a two-way coupling manner with simultaneous and non-iterative calculations (Dukowicz, 1980). It is two-way because the spray carries sufficient momentum to entrain and affect the flow field and the particles are small enough to influence the surrounding gas.

The discrete phase is modeled statistically and not deterministically. This way, as a Lagrangian phase, the particles avoid suffering from numerical diffusion and allow individual attributes to be statistically assigned for each particle. Since the spray is limited to a small part of the domain's mesh and the accuracy is reached with a moderate number of particles, the computational cost is affordable. In addition, identical non-interactive droplets are grouped as parcels (AVL List GmbH, 2021c). Nevertheless, the standard DDM treats the parcels as point sources for mass, momentum and enthalpy in the frame of the Eulerian gas flow field.

The coupling affects momentum, mass and energy transport equations. The atomization also considers drag (arguably the most important force that influences droplet flow), turbulence dispersion, evaporation and breakup. Most of these submodels are additions to DDM's original formulation proposed by Dukowicz (1980). For the current work, the drag law is from Schiller and Naumann (1935), the evaporation model from Dukowicz (1979) and the WAVE breakup model.

The investigation of spray is not the focus of this research. However, it plays important roles in turbulence and combustion too. In relation to turbulence-spray interaction, the individual turbulent eddies influence particle motion and,

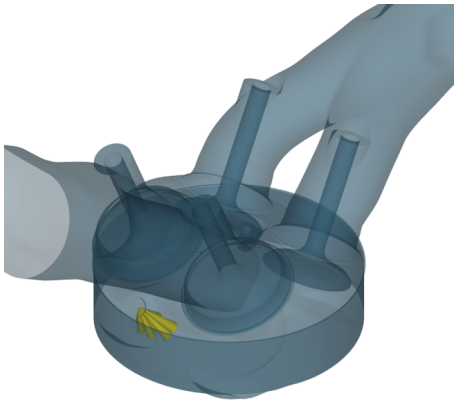

Figure 1: Spray layout. Note that it is located closer to the intake port.

conversely, the particles inertia affect the eddies (AVL List GmbH, 2021c). Due to the large number time and length scales, this interaction is accounted stochastically through the so-called turbulent dispersion submodel. In relation to combustion-spray interaction, the flame promotes evaporation, while spray leads to proper mixture formation. In addition, there are competing effects of cooling due to spray evaporation and flame propagation (Zhou *et al.*, 2021).

3. MATERIALS AND METHODS

The referred AVL FIRE case is a 3D DI-SI ICE transient simulation, composed of intake and exhaust ports, cylinder, spark plug, and valves. That implies that there are moving boundaries and mesh for a complete four-stroke cycle (720 crank angle degrees). The engine has a bore of 81.97 mm, a stoke of 86 mm, and a connecting rod length of 144 mm. The four-stoke cycle is simulated from 172 crank angle degrees (CA) to 892 CA, with the spark ignition occurring at 707 CA. Gasoline is injected at 150 bar with a spray layout that resembles a hexagon with a nozzle hole on each vertex and one in the center. The start of injection (SOI) happens at 430 CA and lasts for 41.8, 51.1 and 60.4 CA, for the 3250, 4000 and 4750 RPM simulations. Figure 1 shows the spray layout. Note that it is located closer to the intake port.

There are two intake and two exhaust valves. Table 1 summarizes important positions, that may be indicated in some further plots. Note that the simulation starts exactly at exhaust valve opening (EVO). For meshing purposes, the valves are considered closed at 0.2 mm of valve lift, to avoid skewed elements between valve and valve seat. The moving mesh is generated using AVL FIRE FAME Engine Plus (FEP), with a volumetric mesh cell size of 1.4 mm, a boundary layer of 0.4 mm made of two layers of cells, and polyhedrical control volumes.

Table 1: Valve lift details

Position	CA [deg]
Exhaust valve opening (EVO)	172.0
Exhaust valve closing (EVC)	396.0
Intake valve opening (IVO)	347.0
Intake valve closing (IVC)	566.0
Max. exhaust lift	280.0
Max. intake lift	454.0

The baseline simulation uses the $k - \zeta - f$ turbulence model, at 4000 RPM. The variations involve changing the turbulence model to $k - \varepsilon$ (keeping the hybrid wall treatment) and/or the rotation to 3250 and 4750 RPM. Concerning the boundary conditions, inlet and outlet mass flow rates, total temperature and pressure were kept the same, only varying the spray module according to the rotation speed. This way, different speeds yield different equivalence ratios. The combustion model is the ECFM-3Z and the spray model is the DDM. Figure 2 shows the boundary conditions. Note that they only affect the simulation between valve openings, and none of them happen from 566 to 892 CA. Besides, for mass flow rate, the sign is relative to the normal of the interface, thus, negative values are entering the domain, while positive values are leaving it.

The fluid in its initial state is taken as ideal-gas air at 1 bar and 1457 K, with a density of 1.19 kg/m^3. The cylinder starts at 1502 K and roughly 4.75 bar. The remaining models involved in the set-up are the laminar flame speed model from Metghalchi and Keck (1982), knock shell model, spherical spark ignition model, NO extended Zeldovich model,

and soot kinetics models. Each simulation ran for roughly 120 hours on a Dell Precision T7500 workstation, which has 48 GB of RAM, and a six-core Intel Xeon X5675 @ 3.07 GHz, running AVL FIRE 2021R1 on Windows 7.

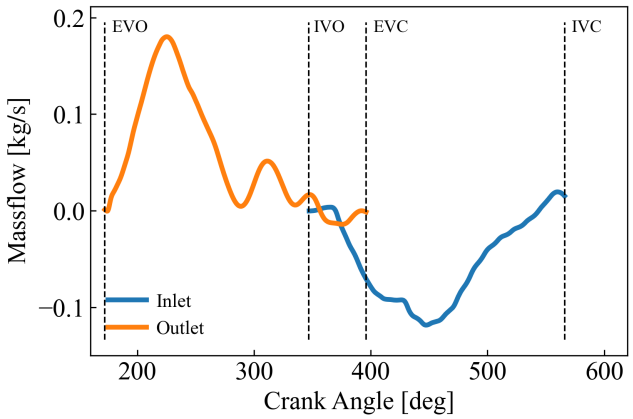

(a) Mass flow rate.

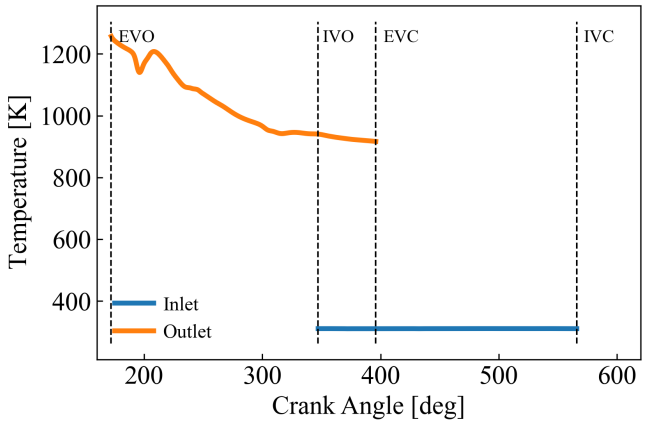

(b) Temperature.

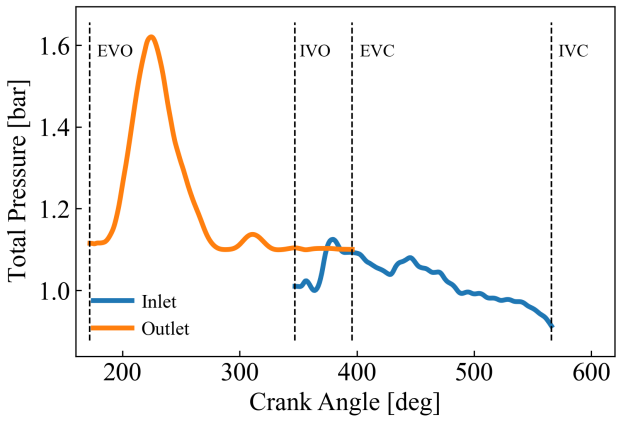

(c) Total pressure.

Figure 2: Inlet and outlet boundary conditions.

4. RESULTS AND DISCUSSION

First of all, the intake/exhaust valves boundary conditions of mass flow, pressure and temperature were kept constant for all simulations. Thus, the change in rotational speed implies a change in equivalence ratio, as a lower speed yields a leaner mixture and a higher speed yields a richer mixture. More precisely, the maximum equivalence ratio (ϕ) for the 3250, 4000, 4750 RPM simulations are 0.87, 1.03, and 1.18, respectively. In addition, by keeping the same spark timing, it is possible that the spark advancement changes its optimum with different speeds. Therefore, the cases should be analyzed within each speed condition for a fairer comparison. Furthermore, the lack of experimental/reference values limits the analysis to a numerical comparison, not being possible to say which model is in better agreement with bench tests.

Table 2 shows the key performance indicators (KPI) for each simulation. There are two parameters to characterize the combustion and four others that are more tangible indicators. MFB stands for mass fraction burnt (in percentage), CBD is the combustion duration/interval between MFBs, IMEP is the indicated mean effective pressure, and BSFC is the brake-specific fuel consumption. The difference column refers to the relative difference (percentage) comparing $k-\varepsilon$ results to $k-\zeta-f$ results. Note that MFB is an instant in time and CBD is a time interval. For this reason, it makes more sense to describe the MFB difference as crank-angle degrees instead of percentage. To aid these comparisons, Tab. 3 shows the mean in-cylinder values of temperature, pressure, heat release and laminar flame speed (LFS), with their correspondent peak magnitudes, when they occurred, and the average value along the four-stroke cycle.

Overall, the higher CBDs in $k-\varepsilon$ simulations show that the combustion takes longer to happen with this model. In particular, the 3250 RPM cases have the largest differences (up to 37.3% in CBD_{10-50}). However, this speed condition should be treated carefully, as the FQ mass fraction (Curran *et al.* (2002) $\mathrm{C}_n\mathrm{H}_{2n}$ species or structures), an intermediate reaction variable that monitors knock, increased for the $k-\zeta-f$ case by approximately two orders of magnitude (Fig. 3a). This increase is not sufficient to produce oscillations in pressure (Fig. 3b), but it caused a notable peak (roughly 14 bar more than $k-\varepsilon$ for the same speed). Therefore, this slight knock occurrence might be the reason for the earlier MFBs

Table 2: Key performance indicators (KPI) calculated for a single four-stroke cycle.

KPI	3250 RPM			4000 RPM			4750 RPM		
	$k-\zeta-f$	$k-\varepsilon$	Diff.	$k-\zeta-f$	$k-\varepsilon$	Diff.	$k-\zeta-f$	$k-\varepsilon$	Diff.
MFB_2 [CA]	719.0	720.9	+1.9	720.6	719.7	-0.9	719.6	719.3	-0.3
MFB_{10} [CA]	724.0	727.2	+3.2	725.8	725.3	-0.5	725.2	724.8	-0.4
MFB_{50} [CA]	731.2	737.0	+5.8	733.4	734.0	+0.6	733.8	734.2	+0.4
MFB_{90} [CA]	739.9	746.8	+6.9	742.8	743.7	+0.9	744.4	745.6	+1.2
CBD_{2-90} [CA]	20.9	25.9	+23.9%	22.2	23.9	+7.9%	24.8	26.3	+6.0%
CBD_{10-50} [CA]	7.1	9.8	+37.3%	7.6	8.7	+15.0%	8.7	9.3	+7.8%
CBD_{10-90} [CA]	15.9	19.6	+23.0%	17.0	18.4	+8.0%	19.2	20.8	+8.1%
IMEP [bar]	12.9	12.5	-3.1%	11.1	11.2	+0.9%	10.1	10.0	-1.0%
Torque [Nm]	47.2	45.8	-3.0%	40.6	41.0	+1.0%	37.1	36.6	-1.3%
Power [kW]	16.1	15.6	-3.1%	17.0	17.2	+1.2%	18.4	18.2	-1.1%
BSFC [g/kWh]	195.4	201.6	+3.2%	227.3	225.0	-1.0%	248.7	252.0	+1.3%

Table 3: In-cylinder mean quantities.

KPI	3250 RPM			4000 RPM			4750 RPM		
	$k-\zeta-f$	$k-\varepsilon$	Diff.	$k-\zeta-f$	$k-\varepsilon$	Diff.	$k-\zeta-f$	$k-\varepsilon$	Diff.
Peak T [K]	2376.2	2329.7	-2.0%	2347.7	2359.6	+0.5%	2400.6	2360.9	-1.7%
When [CA]	741.5	749.0	+7.5	745.0	746.0	+1.0	746.0	747.5	+1.5
Avg. T [K]	927.3	919.6	-0.8%	928.2	929.4	+0.1%	941.2	932.9	-0.9%
Peak p [bar]	72.9	59.0	-19.2%	58.3	56.9	-2.5%	52.3	50.1	-4.1%
When [CA]	736.0	742.0	+6.0	738.4	739.2	+0.8	738.8	739.2	+0.4
Avg. p [bar]	7.3	7.0	-4.6%	6.3	6.3	+0.4	5.8	5.7	-0.6%
Peak ROHR [J/deg]	101.2	75.4	-25.5%	74.8	66.4	-11.2%	63.1	54.8	-13.1%
When [CA]	731.2	738.0	+6.8	731.6	732.4	+0.8	731.8	731.0	-0.8
Accum. HR [J]	1373.8	1381.6	+0.6%	1225.7	1242.3	+1.4%	1118.2	1112.7	-0.5%
Peak LFS [cm/s]	69.6	69.4	-0.3%	77.4	78.8	1.8%	87.1	85.1	-2.3%
When [CA]	750.0	751.0	1.0	748.5	748.0	-0.5	745.5	746.0	0.5
Avg. LFS [cm/s]	21.6	21.8	+0.8%	23.0	23.5	+2.2%	25.4	24.9	-2.1%

and shorter CDBs in this case, possibly due to the increased time for turbulence scales to affect the combustion.

Moreover, the lengthier combustions influence the peak rate of heat release (ROHR), reducing the peak magnitude. Yet, the large changes in peak rate [J/deg] did not reflect much in the accumulated heat release [J]. Figures 3c and 3d show the ROHR and the accumulated heat release along the cycle. Since ROHR resembles a time derivative of heat release, and accumulated heat release is the integration along the cycle, it is possible to see the early increase in accumulated heat release for the 3250 RPM $k-\zeta-f$ case and a later catch-up of $k-\varepsilon$. Similarly, this is also reflected in temperature (Fig. 3e), with an earlier increase for 3250 RPM $k-\zeta-f$ and a delayed increase for $k-\varepsilon$.

As previously mentioned, the ECFM-3Z is a more robust method to predict laminar flame speeds (LFS) than the other CFM models, as it accounts for EGR (Colin *et al.*, 2003). Besides, as a laminar flamelet method, it decouples combustion and chemistry in this respect. Figure 3f shows that there are no major differences in LFS between the turbulence models. Moreover, Tab. 3 shows only slight changes and that, the richer the mixture, the higher the LFS.

Figure 3g shows a normalized turbulence variable that enables a fairer comparison among different engine speeds, and it is the preferred quantity for displaying turbulence intensity (AVL List GmbH, 2021a). It is the average local velocity component due to turbulent fluctuations ($u' = \sqrt{2k/3}$) (Merker *et al.*, 2012), normalized by mean piston velocity (u'/C_m). Notable differences between the turbulence models start after IVO, when the domain is subjected to inflow, but it seems especially affected by the spray, as fuel injection occurs from 430 CA onwards. The $k-\varepsilon$ seems to overpredict the normalized turbulence intensity within that range, with a peak almost matching the one presented nearly to the spark occurrence. Regarding spray and turbulence, this difference might be due to multiphase turbulent mixing, associated to interfacial momentum interaction (Battistoni and Grimaldi, 2012), and to the inherent two-way interaction of the DDM formulation (Dukowicz, 1980). Since this is not the focus of the research, future works should focus on this interaction.

The coherent flame models calculate the flame surface density, which is affected by the turbulence. Besides, a higher flame surface density increases the turbulent flame speed, reducing the burning interval. The results from Tab. 2 suggest that $k-\varepsilon$ produces less turbulence intensity, and therefore, a reduced flame surface density. Note that, even though u'/C_m is higher for $k-\varepsilon$ for most of the cycle, it becomes lower after the ignition (Figs. 3g and 3h).

This is also related to the IMEP, because the reduced flame surface density leads to a slower turbulent flame speed, which alters the pressure peak in location relative to the top dead center (TDC). Note that the differences in the peak location are higher for the lowest RPM (Fig. 3b).

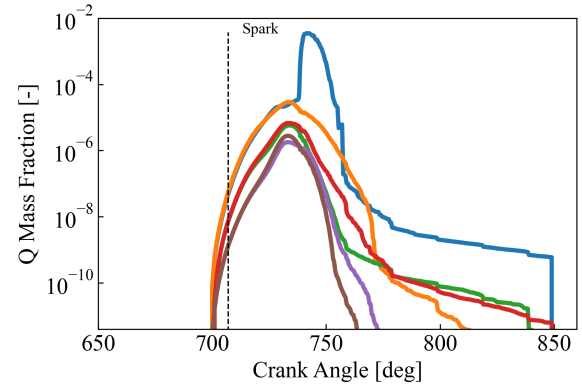

(a) Curran's C_nH_{2n} species or structures. Plot in log-scale.

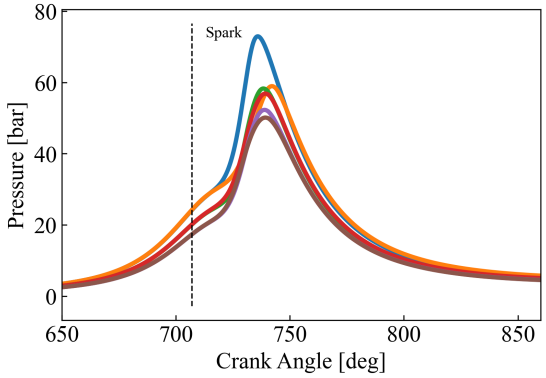

(b) Pressure.

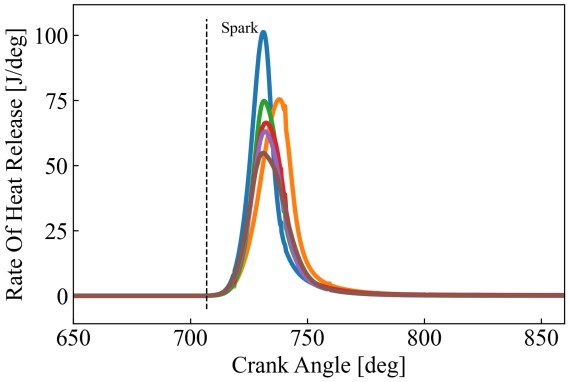

(c) Rate of heat release.

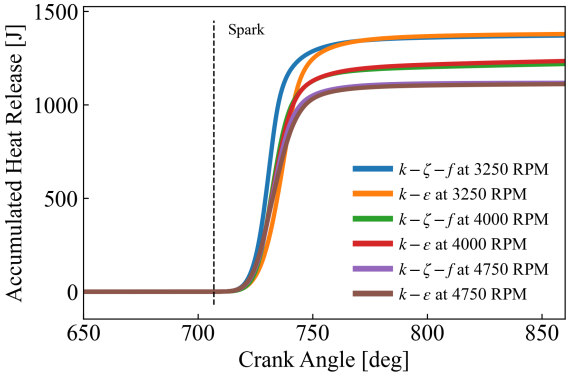

(d) Accumulated heat release.

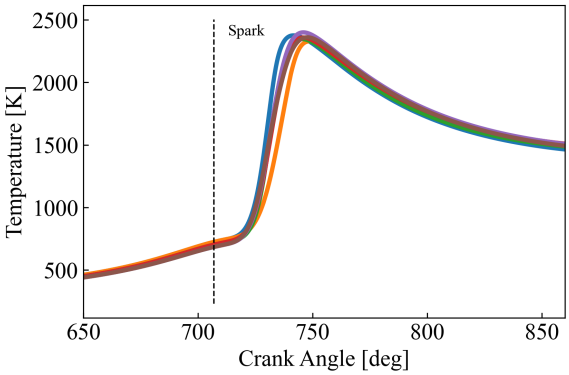

(e) Temperature.

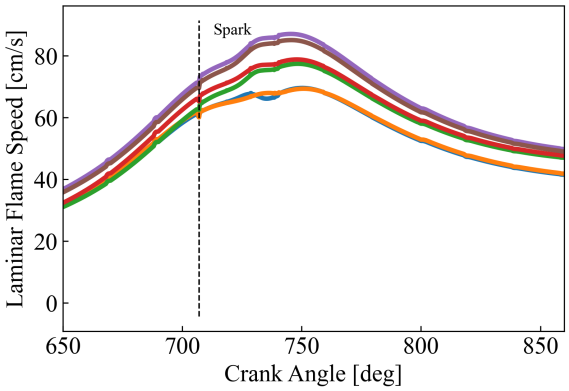

(f) Laminar flame speed.

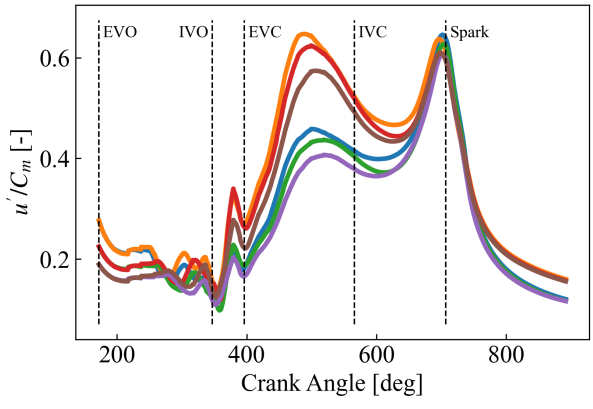

(g) Normalized turbulence: u' divided by piston velocity (C_m).

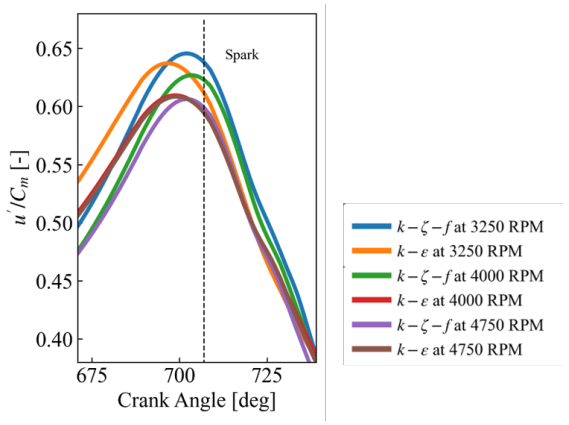

(h) u'/C_m zoom near spark occurrence.

Figure 3: Mean in-cylinder quantities along crank angle.

The same rationale may explain the slight knock at 3250 RPM for $k-\zeta-f$. Since the normalized turbulence is higher, the turbulent flame speed is expected to be higher, which leads to a higher compression of the unburnt mixture prior to the TDC. For the lowest RPM, there is more time for this to happen, leading to ignition. For $k-\varepsilon$, the opposite happens, and associated with lower temperature and pressure, the ignition delay time (IDT) is longer and the ignition that leads to knock does not occur. Conversely, for higher RPMs, there is less time for knock onset.

At last, Fig. 4 shows the top view of MFB_{50} isosurfaces, representing the flame front. Note that it represents different crank-angles but equivalent flame situations (same MFB) and qualitatively depicts the flame front advancement numerically, for visualization purposes. For further studies, it could be compared to experiments to see which model represents best the flame front propagation.

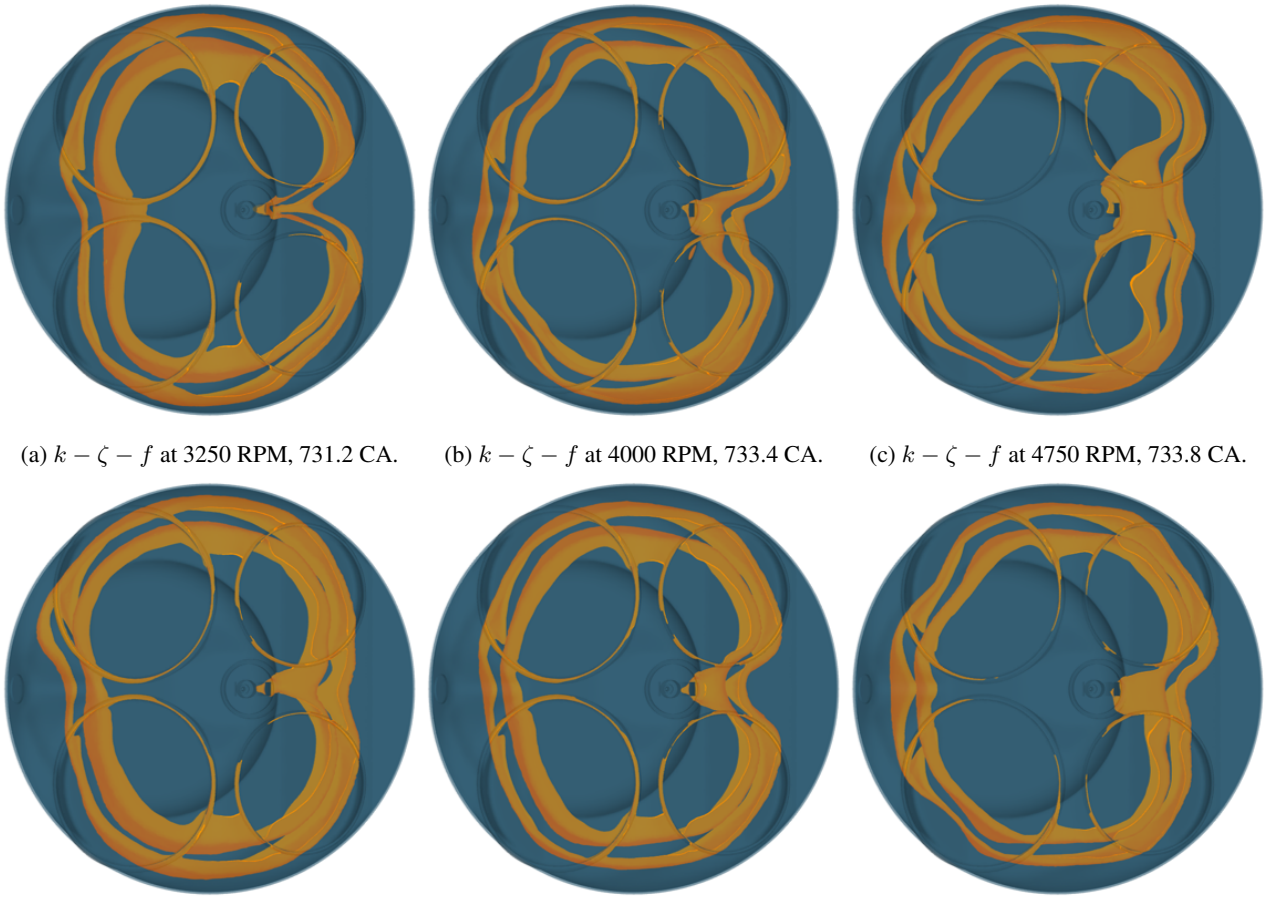

(a) $k-\zeta-f$ at 3250 RPM, 731.2 CA. (b) $k-\zeta-f$ at 4000 RPM, 733.4 CA. (c) $k-\zeta-f$ at 4750 RPM, 733.8 CA.

(d) $k-\varepsilon$ at 3250 RPM, 737.0 CA. (e) $k-\varepsilon$ at 4000 RPM, 734.0 CA. (f) $k-\varepsilon$ at 4750 RPM, 734.2 CA.

Figure 4: Top view of MFB_{50} isosurfaces representing the flame front.

5. CONCLUSION

This work presented a study of turbulence-combustion interactions in 3D computational reactive fluid dynamics (CRFD) simulations of gasoline direct injection (GDI) engines. The cases were simulated in AVL FIRE 2021R1, using the 3-zone extended coherent flame model (ECFM-3Z) for combustion, and the $k-\zeta-f$ and the $k-\varepsilon$ turbulence models, with a hybrid wall formulation. The same mass flow, pressure and temperature intake/exhaust valve boundary conditions with different engine speeds (3250, 4000, 4750 RPM) yielded different stoichiometries, meaning that the simulations should be compared within each speed condition. Furthermore, this might also have changed the optimum spark advancement, as the spark occurrence was kept the same. Besides, the absence of experimental or reference values does not allow to point which model is better, but allows only to point numerically their differences.

Concerning turbulence quantities, the velocity fluctuation normalized by mean piston velocity made the three speed conditions comparable due to this normalization. It showed that $k-\varepsilon$ produced more turbulence during fuel injection, which means that there might be some spray-turbulence interactions as well. As the Discrete Droplet Model (DDM) has a two-way coupling, further work should be done on turbulence-spray interaction. However, after spark, the opposite was verified.

The relation between turbulence and combustion was observed especially for the lowest RPM. The coherent flame

models calculate the flame surface density, which is affected by the turbulence. Besides, a higher flame surface density increases the turbulent flame speed, reducing the burning interval. The results suggested that $k-\varepsilon$ produced less turbulence intensity, and therefore, a reduced flame surface density between the ignition and the top dead center. The unburnt mixture became less compressed and, associated with reduced pressure and temperature led to a longer ignition delay time. On the other hand, $k-\zeta-f$ had opposite results which led to a slight numerical knock detection.

6. ACKNOWLEDGEMENTS

The authors acknowledge the AVL AST University Partnership Program (UPP) for the use and support of AVL-AST software, and the UFSC Joinville IT team (Mr. Kleber Carlos Francisco) for all support given to the LABMCI computer network. The first author acknowledges the financial support granted by the Coordenação de Aperfeiçoamento de Pessoal de Nível Superior – Brasil (CAPES) Master's Fellowship Process No. 88887.658279/2021-00.

7. REFERENCES

AVL List GmbH, 2021a. "FIRE CFD Solver User Manual 2021 R1".

AVL List GmbH, 2021b. "FIRE Combustion 2021 R1".

AVL List GmbH, 2021c. "FIRE Spray 2021 R1".

Battistoni, M. and Grimaldi, C.N., 2012. "Numerical analysis of injector flow and spray characteristics from diesel injectors using fossil and biodiesel fuels". *Applied Energy*, Vol. 97, pp. 656–666. ISSN 0306-2619. doi:10.1016/j.apenergy.2011.11.080.

CFD Online, 2014. "V2-f models". https://www.cfd-online.com/Wiki/V2-f_models.

Colin, O. and Benkenida, A., 2004. "The 3-Zones Extended Coherent Flame Model (Ecfm3z) for Computing Premixed/Diffusion Combustion". *Oil & Gas Science and Technology*, Vol. 59, No. 6, pp. 593–609. ISSN 1294-4475. doi:10.2516/ogst:2004043.

Colin, O., Benkenida, A. and Angelberger, C., 2003. "3d Modeling of Mixing, Ignition and Combustion Phenomena in Highly Stratified Gasoline Engines". *Oil & Gas Science and Technology*, Vol. 58, No. 1, pp. 47–62. ISSN 1294-4475. doi:10.2516/ogst:2003004.

Curran, H.J., Gaffuri, P., Pitz, W.J. and Westbrook, C.K., 2002. "A comprehensive modeling study of iso-octane oxidation". *Combustion and Flame*, Vol. 129, No. 3, pp. 253–280. ISSN 0010-2180. doi:10.1016/S0010-2180(01)00373-X.

Duclos, J.M., Bruneaux, G. and Baritaud, T.A., 1996. "3D Modelling of Combustion and Pollutants in a 4-Valve SI Engine; Effect of Fuel and Residuals Distribution and Spark Location". SAE Technical Paper 961964, SAE International, Warrendale, PA. doi:10.4271/961964.

Duclos, J.M. and Zolver, M., 1998. "3D modeling of Intake, Injection and Combustion in a DI-SI Engine under Homogeneous and Stratified Operating Conditions". *COMODIA*, pp. 335–340.

Dukowicz, J., 1979. "Quasi-steady droplet phase change in the presence of convection". Technical report, United States.

Dukowicz, J.K., 1980. "A particle-fluid numerical model for liquid sprays". *Journal of Computational Physics*, Vol. 35, No. 2, pp. 229–253. ISSN 0021-9991. doi:10.1016/0021-9991(80)90087-X.

Durbin, P.A., 1991. "Near-wall turbulence closure modeling without "damping functions"". *Theoretical and Computational Fluid Dynamics*, Vol. 3, No. 1, pp. 1–13. ISSN 1432-2250. doi:10.1007/BF00271513.

Durbin, P.A. and Reif, B.A.P., 2010. *Models with Tensor Variables*, John Wiley & Sons, Ltd, Chichester, UK, pp. 155–215. ISBN 978-0-470-97207-6 978-0-470-68931-8. doi:10.1002/9780470972076.ch7.

Hanjalić, K., Popovac, M. and Hadžiabdić, M., 2004. "A robust near-wall elliptic-relaxation eddy-viscosity turbulence model for CFD". *International Journal of Heat and Fluid Flow*, Vol. 25, No. 6, pp. 1047–1051. ISSN 0142-727X. doi:10.1016/j.ijheatfluidflow.2004.07.005.

Merker, G.P., Schwarz, C. and Teichmann, R., 2012. *Combustion Engines Development - Mixture Formation, Combustion, Emissions and Simulation*. Springer. ISBN 978-3-642-02951-6.

Metghalchi, M. and Keck, J.C., 1982. "Burning velocities of mixtures of air with methanol, isooctane, and indolene at high pressure and temperature". *Combustion and Flame*, Vol. 48, pp. 191–210. ISSN 0010-2180. doi:10.1016/0010-2180(82)90127-4.

Robert Bosch GmbH, 2022. "Gasoline direct injection". https://www.bosch-mobility-solutions.com/en/solutions/powertrain/gasoline/gasoline-direct-injection/.

Schiller, L. and Naumann, A., 1935. "A Drag Coefficient Correlation". *Zeitschrift des Vereins Deutscher Ingenieure*, , No. 77, pp. 318–320.

Zhou, L., Zhao, W., Luo, K.H., jia, M., Wei, H. and Xie, M., 2021. "Spray–turbulence–chemistry interactions under engine-like conditions". *Progress in Energy and Combustion Science*, Vol. 86, p. 100939. ISSN 0360-1285. doi:10.1016/j.pecs.2021.100939.

8. RESPONSIBILITY NOTICE

The authors are solely responsible for the printed material included in this paper.